Inorganic Chemistry

Article

pubs.acs.org/IC

Characterization of the Copper(II) Binding Sites in Human Carbonic Anhydrase II

Whitnee L. Nettles,[†] He Song,[†] Erik R. Farquhar,[‡] Nicholas C. Fitzkee,*[,†] and Joseph P. Emerson*[,†]

[‡]National Synchrotron Light Source, Brookhaven National Laboratory, Case Western Reserve University Center for Synchrotron Biosciences, Upton, New York 11973, United States

[†]Department of Chemistry, Mississippi State University, Box 9573, Mississippi State, Mississippi 39762-9573, United States

Supporting Information

ABSTRACT: Human carbonic anhydrase (CA) is a well-studied, robust, mononuclear Zn-containing metalloprotein that serves as an excellent biological ligand system to study the thermodynamics associated with metal ion coordination chemistry in aqueous solution. The apo form of human carbonic anhydrase II (CA) binds 2 equiv of copper(II) with high affinity. The Cu^{2+} ions bind independently forming two noncoupled type II copper centers in CA (Cu_A and Cu_B). However, the location and coordination mode of the Cu_A site in solution is unclear, compared to the Cu_B site that has been well-characterized. Using paramagnetic NMR techniques and X-ray absorption spectroscopy we identified an N-terminal Cu^{2+} binding location and collected information on the coordination mode of the Cu_A site in CA, which is consistent with a four- to five-coordinate N-terminal Cu^{2+} binding site reminiscent to a number of N-terminal copper(II) binding sites including the copper(II)-amino terminal Cu^{2+} and Ni^{2+} and copper(II)-β-amyloid complexes. Additionally, we report a more detailed analysis of the thermodynamics associated with copper(II) binding to CA. Although we are still unable to fully deconvolute Cu^{2+} binding data to the high-affinity Cu_A site, we derived pH- and buffer-independent values for the thermodynamics parameters K and ΔH associated with Cu^{2+} binding to the Cu_B site of CA to be 2×10^9 and -17.4 kcal/mol, respectively.

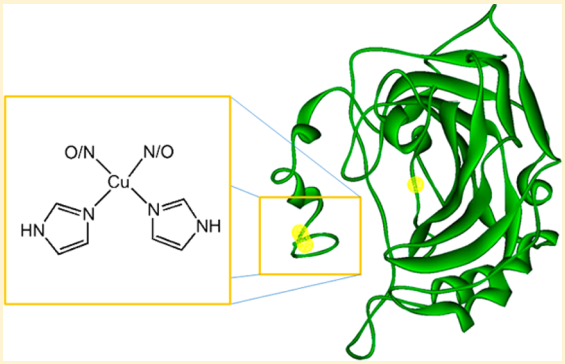

Carbonic anhydrase (CA) is a zinc-dependent metalloenzyme that catalyzes the reversible hydrolysis of carbon dioxide into the bicarbonate ion.[1] The active site of CA contains a mononuclear zinc(II) ion coordinated to three histidine residues (His94, His96, and His119) and one water/hydroxide ligand in a tetrahedral coordination mode. The metal center is kinetically labile, where the metal-free form of CA (apoCA) is relatively stable and easy to generate using pyridine-2,6-dicarboxylic acid (DPA) dialysis.[2] This has allowed for the reconstitution of the three-histidine ($(His)_3$) active site in CA with a range of biologically available metal ions.[3] However, our recent report[6] confirms earlier experimental data that shows that Cu^{2+} binding to CA is more complex than a single site binding event.[3−6] There are two thermodynamically distinctive copper binding sites in apoCA, which we have termed Cu_A and Cu_B. These binding sites have different affinities for Cu^{2+}.[6] Curiously, the lower-affinity site, Cu_B, was found to be the native $(His)_3$ metal binding site of CA, whereas the location and coordination geometry of the high-affinity Cu_A site is unknown. There are several crystallographically characterized Cu-substituted CAs,[3,7,8] but only 1RZC.pdb has a second Cu ion. However, this second Cu^{2+} site is poorly resolved near the N-terminus of the protein, where two conformers within the structure complicates ligand assignments (Figure 1). Here we report our efforts using NMR and X-ray absorption spectroscopy (XAS) techniques to characterize the Cu^{2+} binding sites within CA, specifically, determining the relative location and coordination mode of the high-affinity copper(II) binding site (Cu_A) in CA. Additionally we report the deconvoluted thermodynamic parameters associated with copper(II) coordination to the traditional metal binding site of CA.

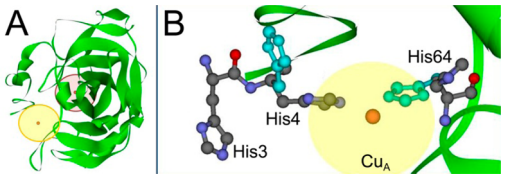

Figure 1. Copper(II) substituted carbonic anhydrase. (A) Location of the crystallographically characterized Cu^{2+} binding sites in Cu_2CA from 1RZC.pdb. Traditional metal binding site in CA is highlighted in pink, where the novel Cu-binding site is shown in yellow. (B) The novel Cu binding site in CA, proposed to be the Cu_A center. His4 and His64 in the Cu_A site are observed to have two different conformers (shown in cyan and colored ball and stick) within 1RZC.pdb.

Received: January 8, 2015
Published: May 26, 2015

ACS Publications © 2015 American Chemical Society

DOI: 10.1021/acs.inorgchem.5b00057
Inorg. Chem. 2015, 54, 5671−5680

MATERIALS AND METHODS

Sample Preparation. CA was overexpressed and purified from the pACA plasmid in *E. coli* BL21(DE3) cells as previously described.[9] The apoCA was prepared by dialyzing native CA against 1 L of 20 mM *N*-(2-acetamido)-2-aminoethanesulfonic acid (ACES) containing 50 mM DPA (pH 7.0). Extra DPA was removed with dialysis of apoCA against 2 L of 20 mM Tris (pH 7.0) buffer, and then with chromatography onto a Sephacryl S-200 size-exclusion column. The concentration of apoCA was determined by UV absorption at 280 nm (ε_{280} = 54 000 M^{-1} cm^{-1}).[10] There are three forms of CA prepared for the study; reconstituted CA (ZnCA, adding 1 equiv Zn^{2+} to apoCA), copper/zinc CA (Cu/ZnCA, addition of 1 equiv Cu^{2+} into ZnCA), and dicopper CA (Cu/CuCA, addition of 2 equiv of Cu^{2+} into apoCA). For NMR experiments, ^{15}N-labeled CA was obtained by growing *E. coli* BL21(DE3)[pACA] in M9 minimal media containing 1 g/L ^{15}N-ammonium chloride as the sole nitrogen source. The ^{15}N-labeled CA species were then purified and prepared as described above.

Nuclear Magnetic Resonance Measurements. All NMR measurements were performed at 298 K on a Bruker 600 MHz Avance III spectrometer with cryoprobe attachment. ^{15}N-labeled samples containing 100 μM CA were prepared in 20 mM phosphate buffer at pH 7.0 (5% v/v D_2O). Three samples were prepared: an apoCA sample containing no metal cofactors, a Cu/ZnCA sample with Zn^{2+} bound in the active site, and a Cu/CuCA sample where Cu^{2+} occupies both the Cu_A and Cu_B sites. $^{15}N-^{1}H$ transverse relaxation optimized spectroscopy (TROSY) spectra were acquired on all samples, and assignments were found to be in excellent agreement with those determined previously.[11] Ambiguous assignments were resolved using a 3D $^{15}N-^{1}H$ mixed-time parallel evolution heteronuclear multiple-quantum correlation nuclear Overhauser effect spectroscopy (HMQC NOESY) with a 150 ms mixing time.[12,13] Addition of paramagnetic Cu^{2+} ions introduced broadening around the Cu_A and Cu_B sites; chemical shifts were largely similar between the three samples, suggesting little to no structural changes in the protein (Figures S1−S3 and Tables S1−S3 found in the Supporting Information).

Paramagnetic relaxation enhancements (PRE; ^{1}H Γ_2 values) were calculated from the difference in ^{1}H TROSY R_2 rates measured in samples with and without Cu^{2+} ($\Gamma_2 = R_2^{PRE} - R_2^{No\ PRE}$). Relaxation rates were measured from a series of interleaved $^{15}N-^{1}H$ TROSY experiments with an additional T_2 relaxation echo introduced during the final readout period as described previously.[14] The relaxation times used were 0, 6, 12, 18, 24, and 36 ms. T_2 values were determined using the relaxation fitting module from Sparky, and uncertainties were determined from the spectral noise.[15] The pH for samples with and without Cu^{2+} and Zn^{2+} were controlled to within 0.2 pH units, and the pH of samples were checked before and after measurement.

Paramagnetic Relaxation Enhancements Data Analysis. To fit the positions of paramagnetic Cu^{2+} ions in the structure of CA, a rigid-body approach was used. Using this approach, the *x*, *y*, and *z* coordinates of one or two Cu^{2+} ions could be optimized in the molecular frame. Proton Γ_2 values were interpreted using a previously determined high-resolution crystal structure of CA (PDB ID 2CBA).[16] Amide protons were added using REDUCE.[17] Optimization coordinates were obtained by maximizing the agreement (minimizing χ^2) between the observed and calculated Γ_2 PRE values. The Solomon−Bloembergen equation was used to calculate Γ_2, assuming each Cu^{2+} site influenced relaxation independently:[18,19]

$$\Gamma_2 = \frac{K}{r_{IS}^6}\left(4\tau_c + \frac{3\tau_c}{1 + (\omega\tau_c)^2}\right) \quad (1)$$

$$K = \frac{1}{15}\left(\frac{\mu_0}{4\pi}\right)^2 (\gamma_I g_S \mu_B)^2 s(s+1) \quad (2)$$

where r_{IS} is the distance between the Cu^{2+} center and the amide proton nucleus, τ_c is the correlation time for the electron−nuclear interaction vector, and ω is the nuclei Larmor frequency in rad s^{-1} (i.e., 3.8 × 10^7 s^{-1} at 600 MHz). The constant K is calculated from the permeability of vacuum μ_0, the gyromagnetic ratio of the ^{1}H nucleus γ_I, the electron spin quantum number s, the electron g-factor g_S, and the electron Bohr magneton, μ_B. The value for τ_c was estimated to be 7 ns from ^{1}H T_2 measurements.[20] Steric overlap was avoided by applying a soft-sphere repulsive potential from the LINUS simulation package.[21] Using these constraints, optimization of the *x*, *y*, and *z* coordinates for both Cu^{2+} nuclei was performed using in-house scripts. The final coordinates were reproducible and did not change significantly when the soft-sphere repulsive potential was applied.

X-ray Absorption Spectroscopy Data Collection and Analysis. The XAS data were collected at beamline X3B of the National Synchrotron Light Source (NSLS) at Brookhaven National Laboratory. A sagitally focusing Si(111) double crystal monochromator was used for energy selection, with a nickel-coated mirror downstream of the monochromator providing harmonic rejection. Cu K-edge XAS spectra were collected in fluorescence mode over an energy range of 8779−9689 eV, using a 31 element Canberra Ge detector. Samples were maintained at a temperature of 20 K under vacuum using a helium Displex cryostat. For internal energy calibration, a copper foil spectrum was collected concomitantly, and its first inflection point was set to 8979 eV.

Two samples (Cu/ZnCA: 1.0 mM in 20 mM ACES with 30% glycerol, and Cu/CuCA: 1.0 mM in 20 mM ACES with 30% glycerol) were transferred to Lucite cuvettes covered with Kapton tape as an X-ray transparent window material and quickly frozen in liquid nitrogen. Three scans were collected and averaged for the Cu/ZnCA sample, and four scans were collected and analyzed for the Cu/CuCA sample. Samples were monitored for evidence of photoreduction, and only those scans showing no photoreduction were included in the final average. Examination of individual scans, averaging, and extraction of the $\chi(k)$ extended X-ray absorption fine structure (EXAFS) was performed using EXAFSPAK.[22] Specifically, a Gaussian function was fitted to the curved pre-edge background (8779−8955 eV), and this function was subtracted from the entire spectrum to remove background absorption. A three-segment spline function having fourth-order components was fit to the background subtracted data (9000−9639 eV) to extract $\chi(k)$. EXAFS analysis was performed using the opt program of EXAFSPAK. Theoretical scattering paths were built from the coordinates of a model of the active site of human CA extracted from the crystal structure coordinates (PDB ID 2CBA),[16] with ab initio phase and amplitude parameters for these paths calculated using FEFF 6.[23] Coordination numbers (n) were varied in integer steps, while the pathlengths (r) and

DOI: 10.1021/acs.inorgchem.5b00057
Inorg. Chem. 2015, 54, 5671−5680

Debye−Waller factors (σ^2) were allowed to freely float. Coordinated His ligands were simulated using a rigid body approximation[24] in which the pathlengths of single- and multiple-scattering paths were constrained to a constant difference from one another. The scale factor was fixed at 0.9 in all fits. E_0, the point at which $k = 0$ Å^{-1}, was defined as 9020 eV, and the edge shift parameter ΔE_0 was allowed to float as a single common value for all shells. Fits to Fourier-filtered first-shell EXAFS data used the goodness-of-fit parameter F', defined as $F' = [\sum(\chi_{exptl} - \chi_{calc})^2]^2/(N_{IDP} - N_{VAR})$, where N_{VAR} is the number of floated variables in the fit, while N_{IDP} is the number of independent data points and is defined as $N_{IDP} = 2\Delta k\Delta r/\pi$. In the latter equation, Δk is the k-range over which the data is fit, while Δr is the back-transformation range employed in fitting Fourier-filtered data. F' provides a useful assessment of the effect of additional shells on improving fit quality (Riggs-Gelasco, 1995 No. 326) The bond-valence sum (BVS) was also used to assess appropriateness of a given first-shell fit. The BVS was calculated using $\sum(\exp[(r_0 - r)/0.37])$, where r_0 is an empirically derived parameter for a given pair of atoms (r_0 = 1.751 for Cu^{2+}−N and 1.649 for Cu^{2+}−O) and r is the actual bond length.[25] For fits to unfiltered EXAFS data, the goodness of fit F factor was defined as $[\sum k^6(\chi_{exptl} - \chi_{calc})^2/\sum k^6\chi_{exptl}^2]^{1/2}$.

UV−vis Spectroscopy and Reactivity Studies. Electronic absorption spectra of Cu/ZnCA and Cu/CuCA were recorded on the OLIS modernized HP 8452A spectrophotometer. Each spectrum was collected on 200 μM protein in 20 mM 4-(2-hydroxyethyl)-1-piperazineethanesulfonic acid buffer at pH 7.4. *para*-Nitrophenyl acetate (pNPA) hydrolysis assays were performed as previously described with some modification.[9,26] All assays were performed in 50 mM Tris buffer at pH 7.4. Reactivity was monitored by the conversion of 10 μM pNPA to *p*-nitrophenol (ε_{404} = 17 300 M^{-1} cm^{-1}) and acetate with 10 μM CA. The pNPA hydrolysis assays were also performed with ZnCA in the presence of copper(II). Reactivity was monitored by the conversion of 10 μM pNPA to *p*-nitrophenol by ZnCA as described above. However, prior to substrate addition aliquots of copper(II) were added to the reaction buffer, and the solution was allowed to incubate for 30 s at 25 °C before the ignition of the reaction. Reaction rates are normalized based zinc(II) content.

Isothermal Titration Calorimetry. Isothermal titratin calorimetry (ITC) experiments were performed at 25 °C, unless indicated otherwise, on a MicroCal VP-ITC calorimeter. Titrations were run in three buffers with different ionization energies (*N*,*N*-bis(2-hydroxyethyl)-2-aminoethanesulfonic acid (BES), 2,2-bis(hydroxymethyl)-2,2′,2″-nitrilotriethanol (Bis-Tris), 2-[(2-hydroxy-1,1-bis(hydroxymethyl)ethyl)amino]-ethanesulfonic acid (TES)), to calculate the number of protons released. A typical experiment consisted of 70 μM apoCA titrated with 1.48 mM $Cu(NO_3)_2$ in TES buffer. All solutions were generated with exactly matched buffers and degassed under vacuum prior to running the experiments. Protein concentrations were calculated from known molar absorptivity of both apoCA and native CA.

ITC data were fit with the Origin software package provided by MicroCal and the CHASM software package. CHASM uses nonlinear least-squares fitting to optimize χ^2 for an arbitrarily specified binding model.[27] Both software packages produced similar optimal values for the stoichiometry (n_{ITC}), change in enthalpy (ΔH_{ITC}), and association constant (K_{ITC}). Comparison of the goodness-of-fit with different models was based on the calculated χ^2 value. Three or more data sets were collected for each type of titration, and the best-fit values were averaged and reported. Estimated uncertainties were calculated using the standard error of the mean. All ITC data that are presented herein are shown as the baseline-adjusted raw data and the peak integrated, concentration-normalized heat of reaction versus the molar ratio of metal ion to protein. The free energy change for the overall equilibrium of each ITC titration, ΔG_{ITC}, was determined from the equilibrium constant obtained for the best fit of the experimental data, K_{ITC}.

RESULTS

Paramagnetic Nuclear Magnetic Resonance Spectroscopy. NMR spectroscopy was used to estimate the location of the Cu^{2+} binding sites within the molecular frame of CA. The spectra of apoCA and ZnCA were obtained to test the suitability of studies involving Cu^{2+}, and assignments were found to be in good agreement with those determined previously (data not shown).[11] The similarity of both spectra suggests that structure of these metal-substituted CAs experience only small structural changes when a foreign metal ion is bound at the active site. In Cu/ZnCA, the traditional metal binding site is occupied by Zn^{2+}, allowing us to directly probe the Cu_A binding site, whereas the Cu/CuCA has both copper ions bound to CA. The paramagnetic Cu^{2+} ions manifest two physical effects in NMR spectra: First, small changes in chemical shifts are expected, corresponding to pseudocontact shifts (PCS) induced by the aniosotropy in the Cu binding site.[18,28] Larger shifts are possible if dramatic structural changes occur with binding. Second, the presence of a paramagnetic electron increases the proton relaxation rate through paramagnetic relaxation enhancement (PRE).[19,29] Both of these effects are observed in Cu/ZnCA, and several residues are broadened beyond detection. Additionally, several chemical shift differences are observed, although these are relatively small (cf. Supporting Information Tables S1−3). Because chemical shift changes could reflect both structural changes as well as PCS contributions, interpreting chemical shift differences can be challenging.[29] PRE rates are more straightforward to interpret, and in this study PREs are used to localize the Cu_A binding site in CA, assuming a rigid-body conformation of the CA structure.

Good agreement is observed between measured PREs and the optimized coordinates of Cu_A (Figure 2). PREs were observed for 181 of 260 residues, and these rates indicate that Cu_A is located in close proximity to the N-terminus of Cu/ZnCA (Figure 3). Coordinate optimization places the Cu_A site close to the site originally observed by Håkansson et al.;[3] His3 and His4 seem like reasonable candidates to coordinate Cu^{2+} in this site. While our experiments cannot determine the precise orientation of the histidine side chains, it seems likely that these residues can reorient to adopt a reasonable metal binding mode. The crystallographically characterized Cu_2CA shows His4 adopting two different conformations within the crystal structure (Figure 1).[3]

PREs were also measured on Cu/CuCA, with the observation that more residues are broadened beyond detection, and chemical shift differences [presumably from pseudocontact shifts (PCS)] are more significant (Supporting Information). For this construct, only 133 PREs could be measured, and because of this there were fewer constraints for determining the location of the Cu_A site. Nevertheless, the Cu/CuCA data set yields a binding site consistent with the Cu/

DOI: 10.1021/acs.inorgchem.5b00057
Inorg. Chem. 2015, 54, 5671−5680

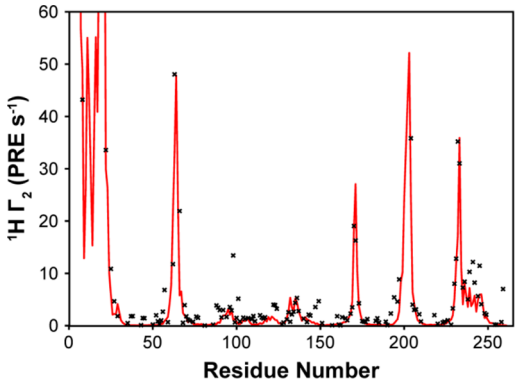

Figure 2. ^{1}H Γ_2 PRE rates in Zn/CuCA. A comparison of observed PRE rates for backbone protons (black points) to the predicted rates (red lines) using the optimal Cu^{2+} coordinates in Zn/CuCA. The coordinates of the optimal Cu center are shown in Figure 3. PREs were measured using the pulse program described by Anthis et al.,[14] and coordinate optimization was performed using the previously determined structure of HCA (PDB ID 2CBA).

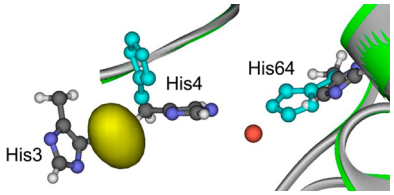

Figure 3. Best-fit coordinates for Cu^{2+} bound to the Cu_A site in CA. The optimized position of the paramagnetic copper(II) ion (Cu_A site) in both Zn/CuCA and Cu_2CA is shown as a yellow spheroid. This region lacks secondary structure; the protein was treated as a rigid body during optimization, and the size and shape of this binding site is representative of the statistical uncertainty in the data. Note the copper atom (orange) described by the previously reported crystal structure of the two copper(II) coordination (1RZC.pdb).

ZnCA data. In this case, the coordinates of the active site Cu_B binding site were fixed to the crystallographic position, while the Cu_B binding site was optimized. The resulting optimized position was less than 2 Å away from the Cu/ZnCA coordinates, indicating a consistent location for this binding site. Importantly, the binding pocket identified by both data sets is consistent, placing the Cu^{2+} in close proximity to the His3 and His4 side chains.

X-ray Absorption Spectroscopy. Since the paramagnetic NMR experiments above have localized copper binding sites near the N-terminal domain of CA (Cu_A) and in the traditional zinc bindings center (Cu_B) and the structure of the native $(His)_3$ metal Cu_B binding site is structurally well-characterized, our main objective is to characterize the local structure of the high-affinity Cu_A site. Figure 4A shows the X-ray absorption near-edge structure (XANES) spectrum of Cu/ZnCA, which is relatively featureless aside from a weak shoulder feature at 8984 eV that can be assigned to a 1s → 4p electronic transition typically seen for Cu^{2+}.[30] The pre-edge peak at 8978 eV associated with a 1s → 3d transition is nearly undetectable. However, the low-energy absorption tail through the 8983–8985 eV region supports a tetragonal Cu^{2+} site in the protein.[31] Further evidence for this notion comes from EXAFS analysis of this sample.

EXAFS analysis typically provides metal–ligand distances within 0.02 Å, identification of donor atoms present ($Z \pm 1$), and an estimate of the coordination number (±25%).[32] Cu/ZnCA exhibited well-defined $k^3\chi(k)$ EXAFS modulations to k = 12 Å^{-1} (Figure 4B), while the Fourier transform shows a single intense peak at r' = 1.5 Å associated with first-shell ligands and a set of weak outer-shell features distributed over r' = 2.2–4.0 Å (Figure 4C). Analysis of the Fourier-filtered first-shell data for Cu/ZnCA indicates that the first shell is fit well by 3–4 N/O scatterers at 1.93 Å (Supporting Information, Table S4), with a fit to 4 N/O ligands favored on the basis of bond-valence sum calculations. Splitting of this shell into two subshells with 2–3 Cu–N/O scatterers at ~2.00 Å and 1–2 Cu–O/N scatterers at ca. 1.90 Å produces a moderate improvement in fit quality. However, the difference in bond lengths was smaller than allowed by the 0.16 Å resolution of the data, while the σ^2 disorder parameter of the shorter subshell was typically large, indicating that two-shell fits cannot be justified with the available EXAFS data. Similar results were obtained for fits to unfiltered data (Table 1). The EXAFS data for Cu/ZnCA also shows evidence for the presence of rigid imidazoles, based on the double-humped feature present at $k \approx 3$–5 Å^{-1} in the k^3-weighted EXAFS as well as the shape of the outer-shell features in the FT from r' = 2.4 to 4.0 Å (Figure 4B,C). Multiple-scattering analysis of these features shows that they are best fit by contributions from two symmetrically bound His ligands (fit 10, Table 1), with fits to other numbers of His ligands producing poorer quality fits. We also performed fits in which the His multiple scattering paths are dependent on the length of the Cu–N_{His} first-shell scatterer.[33] Once again, the best fit involves two His ligands with an average Cu–N_{His} bond length of 1.98 Å and two additional N/O atoms at 1.88 Å (fit 13, Table 1). While EXAFS does not provide direct insight into the origin of the two N/O scatterers at ~1.9 Å, they are likely either solvent or protein-derived ligands (vide infra). XAS data were also collected for Cu/CuCA, which is less informative as the XAS spectra are a weighted average of the structurally distinct Cu_A and Cu_B sites. Thus, precise metrical parameters for the Cu_B site cannot be obtained from direct fits to the EXAFS data. Nevertheless, a first-shell EXAFS analysis of Cu/CuCA shows an average Cu environment of 4–5 N/O scatters at 1.97 Å (Supporting Information, Table S5), suggesting that the Cu_B metal–ligand bond lengths are moderately longer than those of the Cu_A site.

UV–vis Spectroscopy and Reactivity Studies. The UV–vis spectra of Cu/ZnCA and Cu/CuCA are indistinguishable from each other and have no features within the visible region. Both Cu/ZnCA and Cu/CuCA show some hydrolytic activity using the classical *p*-nitrophenylacetate activity assay.[1,34,35] Cu/ZnCA shows 72% of the reactivity of the wild-type ZnCA, whereas the Cu/CuCA has only 28% reactivity. This retained reactivity, especially in the Cu/ZnCA, suggests that many of the mechanistically important amino acids are not dramatically affected by Cu^{2+} coordination to the Cu_A site. These data seem to limit the likelihood that His64 is involved in the Cu_A site. Copper(II) is a known inhibitor of CA,[36] and the inhibition mechanism is likely due to metal substitution into the active site (Cu_B) where copper is apparently less efficient at activating water compared to Zn^{2+}. Additionally, we noted no decrease in *p*-nitrophenylacetate activity of ZnCA with increasing amounts of copper(II) in solution under these conditions (Supporting Information, Figure S4.)

Isothermal Titration Calorimetry. We have reported preliminary ITC results of Cu^{2+} binding to apoCA previously.[6]

DOI: 10.1021/acs.inorgchem.5b00057
Inorg. Chem. 2015, 54, 5671–5680

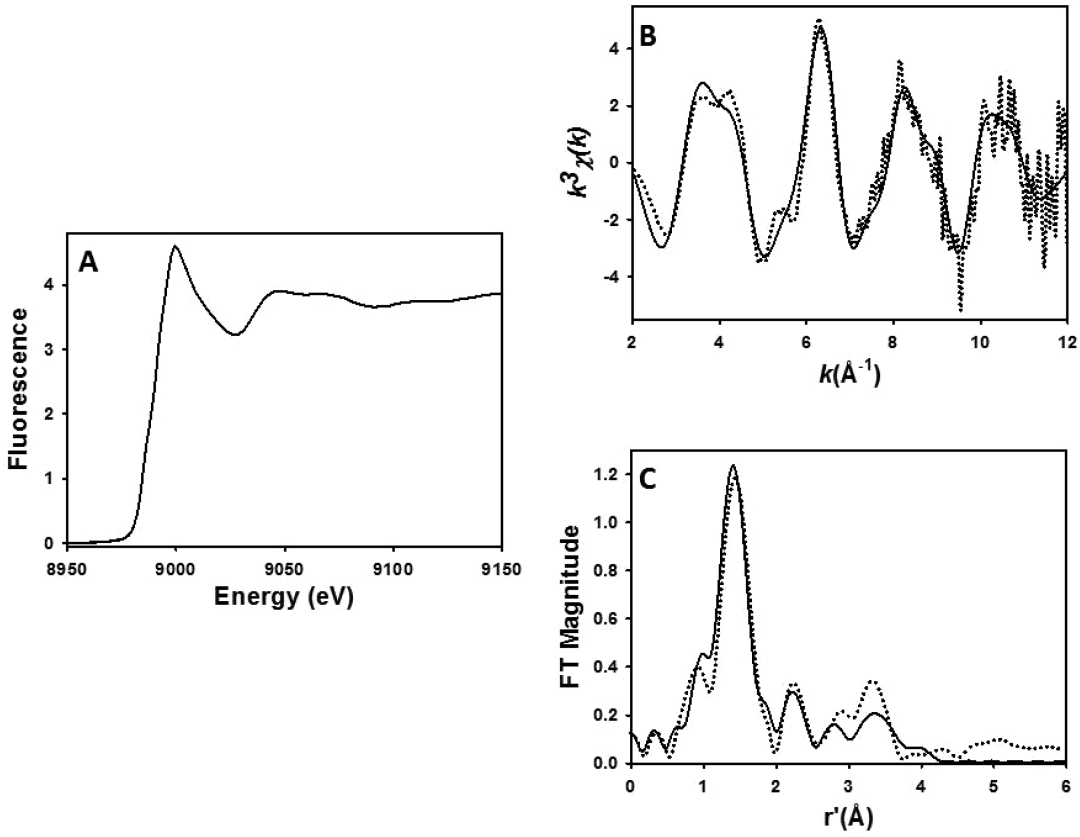

Figure 4. XANES spectra (A), unfiltered $k^3\chi(k)$ EXAFS spectra (B), and the Fourier transform (C); k = 2.0−12.0 Å^{-1} for Cu/ZnCA ensuring Cu^{2+} coordination to the Cu_A site. Experimental data are represented by dotted lines, while best fits (given in bold in Supporting Information, Table S5) are shown as solid black lines.

However, recently new data has become available that allows a further deconvolution of Cu^{2+} binding data,[37,38] which allows for the determination of specific parameters from the equilibria associated with Cu^{2+} binding to apoCA. A representative isotherm for the addition of Cu^{2+} to apoCA in TES, the integrated enthalpy change data, and nonlinear regression fit are shown in Figure 5. The ITC titration of Cu^{2+} into apoCA yields a complex set of equilibria that can be readily fit to a two-site binding model. Similar experiments were performed in three different buffers yielding the experimentally measured ITC data (K_{ITC}, ΔH_{ITC}) shown in Table 2. The ΔG_{ITC} and $-T\Delta S_{ITC}$ terms can be easily derived from the following equations, respectively, $\Delta G_{ITC} = -RT \times \ln(K_{ITC})$ and $\Delta G_{ITC} = \Delta H_{ITC} - T\Delta S_{ITC}$. A high-affinity Cu_A binding site coordinates a stoichiometric amount of Cu^{2+} with an equilibrium constant (K_{ITC}) of ∼1.8 × 10^8. This value is nearly 1000 times higher than the K_{ITC} for the low-affinity Cu_B site (1.4 × 10^5). The two sites elucidated via $Cu(NO_3)_2$ titration into ZnCA were described previously.[5] Note that the K_{ITC} is the product of the K_a for metal ion binding to apoCA and the K_d of the metal−buffer complex. The K_{ITC} values measured for the two Cu^{2+} binding sites can be compared but require more analysis to achieve a pH and buffer-independent binding constant.

Similar to the K_{ITC} discussed above, the change in enthalpy measured from the ITC experiments (ΔH_{ITC}) is the sum of reaction enthalpies linked to the metal binding process. Upon metal binding, pK_a values from local ionizable groups will change. Typically this is observed as a loss of proton density to the solvent, where the buffer ionization also generates added heat-based ionization energy ($\Delta H_{H\text{-}buffer}$). This notion is evident from the linear dependence of the addition of observed enthalpy from ITC and metal−buffer interaction enthalpy (ΔH_{ITC} + $\Delta H_{Cu\text{-}buffer}$) versus the change in enthalpy of ionization for each buffer ($\Delta H_{H\text{-}buffer}$) as shown in Figure 6. This linear relationship can be fit by eq 3, where $\Delta H_{H-buffer}$, $\Delta H_{Cu-buffer}$, ΔH_{H-CA}, and ΔH_{CuCA} are heats associated with proton and metal binding to the buffer and apoCA with n_P as the number of protons released.[9]

$$\Delta H_{ITC} + \Delta H_{Cu-buffer} = n_P(\Delta H_{H-buffer}) + (\Delta H_{CuCA} - n_P\Delta H_{H-CA}) \quad (3)$$

By performing our reactions in 100 mM buffer fixed at pH 7.4, a single speciation of buffer−copper complex can be assumed. The high concentration of buffer allows for only a slight reduction in the buffering capacity from copper−buffer complex formation while still maintaining a set pH. Studying the metal binding process in multiple buffers and plotting the metal−buffer and observed enthalpy versus the ionization enthalpy, we can estimate the proton release of the reaction, as described above. As a result, the slope of this curve suggests ∼1.8 protons are displaced by Cu^{2+} binding from the high-affinity Cu_A site, whereas 0.8 protons are released from the Cu_B site, shown in Figure 6.

The ITC experiment measures the total heat upon addition of titrant; however, there are competitive binding equilibriums associated with metal binding events. In this case, two competing equilibria are involved, buffer competing with protein for access to the metal as well as protons competing with metal for the protein.[37] By utilizing these well-understood

DOI: 10.1021/acs.inorgchem.5b00057
Inorg. Chem. 2015, 54, 5671−5680

Table 1. EXAFS Analysis of Unfiltered Data of Cu/Zn−CA[a]

	Cu−N/O			Cu···C(His)					
fit	n	R	σ^2	n	r	σ^2	F	F-factor	ΔE_0
1	3	1.92	2.9				254.5	0.550	−13.9
2	4	1.92	4.8				234.4	0.539	−14.1
3	5	1.92	6.4				242.9	0.548	−14.9
4	6	1.92	8.0				261.4	0.568	−15.6
5	7	1.92	9.4				286.7	0.595	−16.4
6	4	1.92	4.6	2C	2.86	2.0	193.2	0.489	−14.0
7	4	1.92	4.6	4C	2.86	5.3	187.0	0.481	−13.9
8	4	1.92	4.6	6C	2.87	8.0	189.3	0.484	−13.6
9	4	1.92	4.6	1His	2.86	1.5	155.0	0.438	−14.6
					4.03	0.8			
					4.06	0.8			
					2.86	5.2			
10	4	1.92	4.6	2His	4.04	4.9	143.2	0.420	−14.0
					4.07	4.9			
					2.87	8.2			
11	4	1.92	4.6	3His	4.05	7.9	146.7	0.426	−13.7
					4.08	7.9			
					2.87	11			
12	4	1.92	4.6	4His	4.05	10	158.1	0.442	−13.6
					4.08	10			
13	2	1.88	2.9	2His	1.98	6.0	129.0	0.394	−12.5
					2.88	5.9			
					4.04	5.9			
					4.07	5.9			
14	1	1.88	0.6	3His	1.96	6.5	130.6	0.402	−4.73
					2.89	9.0			
					4.06	9.0			
					4.08	9.0			

[a] r is in units of Å; σ^2 is in units of 1×10^{-3} Å^2; ΔE_0 is in units of eV. All fits are to unfiltered EXAFS data over k = 2.0−12.0 Å^{-1}. In fits 9−12, the His imidazoles were treated as a rigid body, and included single scattering paths for Cu−Ca and both three- and four-body paths involving Cu−Ca−Cβ/Nβ (Cβ and Nβ are the more distant atoms of the imidazole). Fits 13−14 also included a three-body path for Cu−N_{His}−Ca. The path lengths for the rigid imidazole were constrained to a constant difference from one another, and σ^2 was constrained to be identical for paths containing the same set of atoms.

processes the buffer- and pH-independent thermodynamic values of copper binding to apoCA could be derived from a thermodynamic cycle in a similar strategy to those previously reported.[39] The overall equilibrium measured in the ITC is a summation of the dissociation of the Cu^{2+}-buffer complex and the association of Cu^{2+} to the apoCA, along with the dissociation of protons from the CA and the association of protons to the bulk buffer. Although the equilibrium constants associated with a number of Cu−buffer species have been previously reported,[40−42] other thermodynamic parameters where characterized using ethylenediaminetetraacetic acid displacement experiments (Supporting Information, Figure S5 and Table S6). To fully understand the thermodynamics associated with copper binding, the coordination environment of the copper ions needs to be structurally characterized. Without specific information regarding the coordination of the metal ion, as is the case for the Cu_A site, we cannot complete a full analysis of the thermodynamic parameters with the binding event.

At the traditional $(His)_3$ Cu_B site, the pK_a values associated with the copper-bound histidine ligands (His94, His96, and His119) are less than 6 in apoCA; thus, it seems unlikely for deprotonation to occur from the side-chain residues.[9] The other reasonable option would be that the protons could be released from copper-bound water molecules.[6,43] The pK_a of copper-bound water is unknown, but we can back calculate the value from experimental data. Given there are two labile coordination sites in the Cu_B site that are likely filled by water,[3] and 0.8 protons are released during our experiments at pH 7.4, we can establish an average pK_a of ∼8.0 for the copper-bound waters. The protons released from CA as metal ion binds will be released into the bulk solvent and interact with buffer, and the thermodynamic terms associated with the ionization of various buffers are well-known.[40,41,44] Thus, a release of 0.8 protons from CA is shown to change the ionization states of the buffer. Using the data collected from the complex equilibrium and the three previously described simpler equilibria, we can estimate the thermodynamic parameters associated with Cu^{2+} binding to apoCA with the disentanglement of the linked equilibria associated with this system.

In the traditional $(His)_3$ metal binding site (Cu_B) binds Cu^{2+} with a higher affinity than Zn^{2+}, which follows the Irving Williams series.[9] The average condition-independent change in enthalpy (ΔH) of this binding event is calculated to be −17.4 kcal/mol, and the related change in entropy is estimated to be −13.1 cal/mol/K (where $-T\Delta S$ = 3.9 kcal/mol). The Cu^{2+} binding event to the Cu_B site is highly enthalpy driven. However, this process suffers a slight entropic penalty, which is likely due to increasing the order of the active site, which is likely derived from the ordering of water molecules and

DOI: 10.1021/acs.inorgchem.5b00057
Inorg. Chem. 2015, 54, 5671−5680

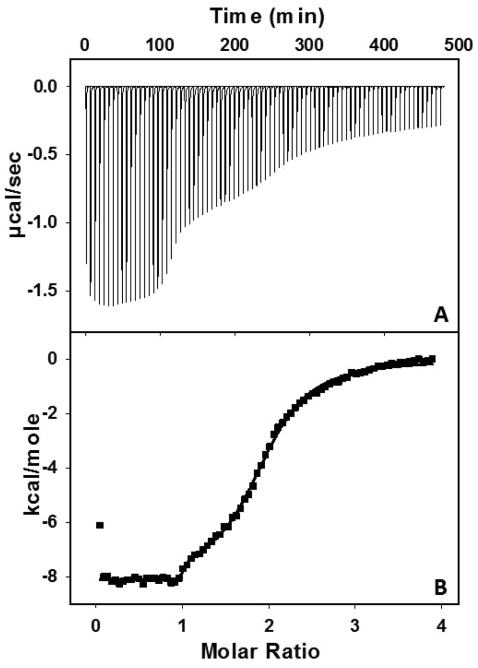

Figure 5. ITC data of copper binding to apoCA. (A) Raw data from the titration of a 1.5 mL cell containing 70 μM apoCA was titrated with 80 × 3 μL of 1.48 mM $Cu(NO_3)_2$ in 100 mM TES at pH 7.4. (B) Integrated isotherm and the best associated fit for a two-site binding model. The average thermodynamic parameters associated with Cu^{2+} binding to apoCA are reported in Table 1.

formation of hydrogen bonding networks between second sphere residues and coordination residues, and/or the coordination of the three His residues (His94, His96, and His119). This analysis generates significantly different thermodynamic parameters than were previously reported for Cu^{2+} binding to apoCA,[43] where the metal–buffer interactions were not considered as part of their analysis.

DISCUSSION

CA is an excellent model protein for biophysics, bioanalysis, the physical-organic chemistry of inhibitor design, and medicinal chemistry.[1] This designation holds true when considering the thermodynamic data discussed here for the classic three-His metal binding site and the active site of CA (described here as the Cu_B site). Our analysis yields terms consistent with the strong association constant observed for Cu^{2+} binding to the Cu_B site of apoCA ($K \approx 2 \times 10^9$), where the corresponding condition-independent thermodynamic terms ΔG°, ΔH, and $-T\Delta S$ terms are −13.5, −17.4, and +3.9 kcal/mol, respectively. These values compare well with the thermodynamic terms associated with the enthalpy-driven Zn^{2+} binding to apoCA reported earlier.[9] The Cu^{2+} and Zn^{2+} binding data appear to

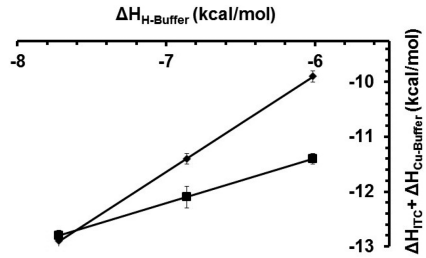

Figure 6. Plot of the addition of observed enthalpy from ITC and metal-buffer interaction enthalpy (ΔH_{ITC} + $\Delta H_{Cu\text{-}buffer}$) vs buffer ionization enthalpies ($\Delta H_{H\text{-}buffer}$) in various buffers at pH 7.4. Values for ΔH_{ITC}, $\Delta H_{Cu\text{-}buffer}$, and $\Delta H_{H\text{-}buffer}$ in various buffers are listed in Tables 3 and 4. Symbols: ◆ indicates Cu_A; ■ indicates Cu_B, and the linear regression values are $y = 1.76x - 0.68$, $R^2 = 0.99$ and $y = 0.82x - 6.46$, $R^2 = 0.99$, respectively.

Table 3. Thermodynamic Cycle for Cu^{2+} Binding to the Cu_B Site in apoCA in 100 mM TES, pH = 7.4

eq	reaction	coeff	ΔH (kcal/mol)	ΔG° (kcal/mol)
	$Cu(TES)^{2+} + (H^+)_{0.8}CA \rightarrow CuCA^{2+} + 0.8\ H^+TES + 0.3\ TES$		−8.0[a]	−7.1[a]
1	$Cu(TES)^{2+} \rightarrow Cu^{2+} + TES$	1	4.8[b]	5.3[c]
2	$H^+CA \rightarrow H^+ + CA$[d]	0.8	13.5[e]	9.3[f]
3	$TES + H^+ \rightarrow H^+TES$	0.8	−7.8[g]	−10.1[g]
4	$Cu^{2+} + CA \rightarrow CuCA^{2+}$	1	−17.4	−12.9

[a]From Table 1. [b]From Supporting Information, Table S6. [c]Reference 37. [d]The reaction can be written as $(His)_3Cu\text{-}(H_2O)_2 \rightarrow 0.2(His)_3Cu\text{-}(H_2O)_2 + 0.8(His)_3Cu\text{-}(OH^-)(H_2O) + 0.8H^+$. [e]Reference 6. [f]$pK_a$ of copper bound water is 8.0 from $\Delta G^\circ = -RT \times \ln(K_a)$. [g]Ionization of TES buffer from ref 52.[59]

follow the Irving–Williams series,[45] a classical observation on the stability of transition metal complexes. In this specific example, however, there are dramatic differences in the metal coordination geometries of Cu^{2+} and Zn^{2+} in the active site of CA. Cu^{2+} favors a trigonal pyramidal geometry in this system, whereas Zn^{2+} binds in a tetrahedral geometry.

Combining the data reported above with our previously published data we can draw two conclusions regarding the Cu_A site in copper-substituted CA. (A) The paramagnetic NMR data shown above locates the Cu_A site in both Cu/ZnCA and Cu_2CA in the unstructured N-terminal region of the protein. (B) The XAS data on the Cu_A site is fully consistent with a four-coordinate tetragonal Cu^{2+} site, with two Histidine ligands. The Cu_A site appears to be a member of a growing number of proteins and peptides that have been found to have an N-terminal Cu^{2+} binding site. The previously reported electron paramagnetic resonance spectra for the Cu_A site and binding isotherms are strikingly comparable to those observed in proteins with N-terminal copper binding sites, such as the amino terminal Cu^{2+} and Ni^{2+} (ATCUN) binding motif found

Table 2. Experimental Values for $Cu(NO_3)_2$ Binding to apoCA from ITC Experiments in 100 mM Buffer at pH 7.4

site	buffer	n_{ITC}	K_{ITC}	ΔH_{ITC} (kcal/mol)	ΔG_{ITC} (kcal/mol)	$-T\Delta S_{ITC}$ (kcal/mol)
A	BES	0.9	2.8 (±2.0) × 10^8	−4.2 ± 0.1	−11.4 ± 0.5	−7.2 ± 0.5
	Bis-Tris	1.0	7.2 (±2.8) × 10^7	−4.1 ± 0.1	−10.7 ± 0.2	−6.6 ± 0.2
	TES	1.0	1.9 (±0.5) × 10^8	−8.1 ± 0.1	−11.3 ± 0.1	−3.2 ± 0.1
B	BES	1.1	2.4 (±0.8) × 10^5	−5.7 ± 0.1	−7.3 ± 0.2	−1.6 ± 0.2
	Bis-Tris	1.0	1.7 (±0.3) × 10^4	−4.8 ± 0.2	−5.8 ± 0.1	−1.0 ± 0.2
	TES	1.0	1.6 (±0.3) × 10^5	−8.0 ± 0.1	−7.1 ± 0.1	0.9 ± 0.1

DOI: 10.1021/acs.inorgchem.5b00057
Inorg. Chem. 2015, 54, 5671−5680

Table 4. Summary of pH- and Buffer-Independent Thermodynamic Values for Cu^{2+} Binding to ApoCA

Cu_B [$(His)_3$-Cu^{2+}]	BES	4.1 (±0.8) × 10^9	−17.4 ± 0.1	−13.1 ± 0.2	4.3 ± 0.2
	bis-tris	4.9 (±0.3) × 10^{10}	−17.4 ± 0.2	−14.6 ± 0.1	2.8 ± 0.2
	TES	2.7 (±0.3) × 10^9	−17.4 ± 0.1	−12.9 ± 0.1	4.5 ± 0.1
	average	1.9 × 10^{10}	−17.4	−13.5	3.9

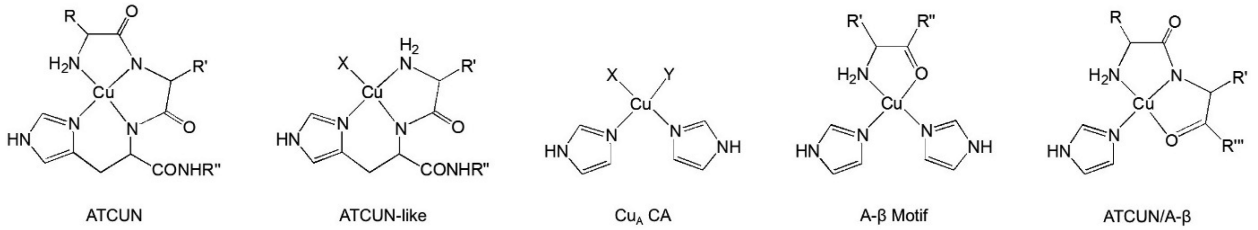

Figure 7. A comparison of the four possible structures of the Cu_A site. The ATCUN having an N-terminal binding, two backbone amides, and histidine coordinated with the Cu ion. The ATCUN-like have an N-terminal binding, one backbone amide, a histidine, and another N/O donor ligand. The expected structure of the Cu_A site. The A-β structure with an N-terminal binding, carboxyl oxygen coordination, and two histidines. The final possibility is the ATCUN/A-β with an N-terminal binding, backbone amide, carboxyl oxygen, and histidine coordination to the copper ion.

in serum albumin and in a range of other small bioactive peptides,[6,46−50] and the Cu-binding site found in some amyloid β-peptide complexes (A-β),[51,52] as shown in Figure 7.

The ATCUN motif is traditionally thought to coordinate copper through an imino nitrogen of His side chain, two deprotonated backbone amides, and the N-terminal amine. The sequence requirement for this binding mode is an XXH sequence at the N-termini, which is highly consistent with the N-terminal domain of the recombinant CA. The ATCUN motif has a distinctive visible absorption spectrum and has been shown to release three protons as metal coordinates (where the N-termini and two backbone amides are deprotonated.)[44] This is inconsistent with our results reported here, where the Cu_A site has no distinctive visible spectra and we only see ∼2 H^+ released as Cu^{2+} binds to the Cu_A site in CA. Additionally, we attempted a range of Ni^{2+} titrations with apoCA, which consistently show only one coordination event in apoCA (data not shown). This is consistent with the ITC data and structural characterization of the NiCA complex that has Ni^{2+} coordinated to the traditional $(His)_3$ active site of CA.[3,43] From these data, we hypothesize that the Cu_A site is not a traditional ATCUN binding domain, although some structural features of the two may still be similar.

Interestingly there is also an ATCUN-like binding mode, which was previously described for the short peptide GHK.[44] Here the same imino nitrogen of a His side chain is coordinated, along with the N-terminal amine, but only one amide nitrogen is coordinated from the first three amino acids. The final coordination site is an unknown ligand, predicted to be an oxygen atom (water/buffer).[53] There has been ITC analysis of Cu^{2+} binding to both the GHK and DAHK (ATCUN-like motif and ATCUN motif, respectively); unfortunately, however, the full thermodynamic analysis was never performed for these two motifs. Upon coordination of copper(II) to the GHK peptide, two protons are released, and the proton release to the ATCUN motif was three protons. Our ITC analysis of copper(II) coordination to the Cu_A site shows a similar proton release to the ATCUN-like motif (Figure 7).

While the Cu_A site may indeed be the ATCUN-like binding motif described, there is yet another reasonable possibility for the coordination site. The β-amyloid (A-β) coordination to copper(II) shows many similarities to our Cu_A site. It has been reported the coordination of Cu^{2+} to different lengths of the β-amyloid;[54] we can see more similarities in the spectra between the Cu_A site and the β-amyloid (A-β) coordination to copper(II), when compared with the ATCUN-like XAS reported in Hureau et al.[53] The similarities between the two spectra include two His residues and two oxygen or nitrogen donors. As can be deduced, the XAS data fit with both the ATCUN-like binding motif and the A-β coordination sphere described previously. From the above spectroscopic studies, it is reasonable to say that the N-terminus region of CA has a coordination environment that is similar to the ATCUN-like and the A-β_{5-23} or a combination of the two.

The data are consistent with the Cu_A binding two His side-chain residues and an N-terminal amine. The N-terminal amine of CA is expected to have a $pK_a \approx 9.7$,[55] where the N-terminus will lose a proton to coordinate to the Cu^{2+} center. This is the only proton than can be assumed from the data. One option for the other 0.8 protons is the coordination of one of four His residues in close proximity to the Cu^{2+} with pK_a values near 7.1, giving a similar structure to the A-β.[56,57] The next possibility is the proton coming from a backbone amide, modeling the ATCUN-like motif or ATCUN/A-β motif, or a different coordinating moiety such as a solvent molecule (water or buffer). Without a reliable structure a full thermodynamic analysis is impossible, and the calculated pH- and buffer-independent thermodynamic parameters for this site cannot be reported at this time.

It is unclear why CA has the Cu_A site in addition to the more traditional metal-binding active site. We found no reactivity associated with the Cu_A site, which could suggest that it has no accessible or labile coordination sites,[6] and this could imply that the physiological role may be related to just sequestering adventitious Cu^{2+}. Copper(II) has been reported to inhibit ZnCA previously,[36,58] although these studies were performed at relatively high concentrations of Cu^{2+}. Perhaps the high-affinity Cu_A binding site and the relatively high cellular expression of CA could work together to limit the levels of adventitious Cu^{2+} during periods of copper dis-homeostasis. This notion is supported by our reactivity studies that suggest there is limited effect of up to 2 equiv of Cu^{2+} in solution to the ZnCA catalyzed *p*-nitrophenylacetate hydrolysis activity. The Cu_A site seems to effectively defend the native zinc(II)−$(His)_3$ active site of CA as well as other metalloproteins from Cu^{2+} displacement, and in some cases inactivation. In the end it is

DOI: 10.1021/acs.inorgchem.5b00057
Inorg. Chem. 2015, 54, 5671−5680

not clear what role the Cu_A site is playing in vivo; however, it is clear that this is a novel high-affinity Cu^{2+} binding domain in CA that raises new questions about this old protein.

■ ASSOCIATED CONTENT

Supporting Information

PRE rates and model fitting, chemical shift changes, and tabulated NMR data. The Supporting Information is available free of charge on the ACS Publications website at DOI: 10.1021/acs.inorgchem.5b00057.

■ AUTHOR INFORMATION

Corresponding Authors

*E-mail: jemerson@chemistry.msstate.edu. (J.P.E.)
*E-mail: nfitzkee@chemistry.msstate.edu. (N.C.F.)

Notes

The authors declare no competing financial interest.

■ ACKNOWLEDGMENTS

The authors thank Mississippi State Univ. for start-up funding to J.P.E. and N.C.F. All XAS experiments were performed at beamline X3B of the NSLS at Brookhaven National Laboratory. Beamline X3B is operated by the Case Center for Synchrotron Biosciences, supported by National Institutes of Health NIBIB Grant No. P30-EB-009998. NSLS is supported by the United States Department of Energy, Office of Science, Office of Basic Energy Sciences, under Contract No. DE-AC02-98CH10886.

■ REFERENCES

(1) Krishnamurthy, V. M.; Kaufman, G. K.; Urbach, A. R.; Gitlin, I.; Gudiksen, K. L.; Weibel, D. B.; Whitesides, G. M. *Chem. Rev.* **2008**, *108*, 946−1051.
(2) Hunt, J. B.; Rhee, M.-J.; Storm, C. B. *Anal. Biochem.* **1977**, *79*, 614−617.
(3) Håkansson, K.; Wehnert, A.; Liljas, A. *Acta Crystallogr., Sect. D: Biol. Crystallogr.* **1994**, *50*, 93−100.
(4) Wischeler, J. S.; Heine, A.; Klebe, G. *Curr. Chem. Biol.* **2011**, *5*, 1−8.
(5) Hunt, J. A.; Ahmed, M.; Fierke, C. A. *Biochemistry* **1999**, *38*, 9054−9062.
(6) Song, H.; Weitz, A. C.; Hendrich, M. P.; Lewis, E. A.; Emerson, J. P. *J. Biol. Inorg. Chem.* **2013**, *18*, 595−598.
(7) Cox, J. D.; Hunt, J. A.; Compher, K. M.; Fierke, C. A.; Christianson, D. W. *Biochemistry* **2000**, *39*, 13687−13694.
(8) Jude, K. M.; Banerjee, A. L.; Haldar, M. K.; Manokaran, S.; Roy, B.; Mallik, S.; Srivastava, D. K.; Christianson, D. W. *J. Am. Chem. Soc.* **2006**, *128*, 3011−3018.
(9) Song, H.; Wilson, D. L.; Farquhar, E. R.; Lewis, E. A.; Emerson, J. P. *Inorg. Chem.* **2012**, *51*, 11098−105.
(10) Alexander, R. S.; Kiefer, L. L.; Fierke, C. A.; Christianson, D. W. *Biochemistry* **1993**, *32*, 1510−1518.
(11) Venters, R. A.; Farmer, B. T., II; Fierke, C. A.; Spicer, L. D. *J. Mol. Biol.* **1996**, *264*, 1101−1116.
(12) Fitzkee, N. C.; Masse, J. E.; Shen, Y.; Davies, D. R.; Bax, A. *J. Biol. Chem.* **2010**, *285*, 18072−18084.
(13) Ying, J.; Chill, J. H.; Louis, J. M.; Bax, A. *J. Biomol. NMR* **2007**, *37*, 195−204.
(14) Anthis, N. J.; Doucleff, M.; Clore, G. M. *J. Am. Chem. Soc.* **2011**, *133*, 18966−18974.
(15) Goddard, T. D.; Kneller, D. G. *SPARKY 3;* University of California.
(16) Håkansson, K.; Carlsson, M.; Svensson, L. A.; Liljas, A. *J. Mol. Biol.* **1992**, *227*, 1192−1204.
(17) Word, J. M.; Lovell, S. C.; Richardson, J. S.; Richardson, D. C. *J. Mol. Biol.* **1999**, *285*, 1735−1747.
(18) Bertini, I.; Luchinat, C.; Rosato, A. *Prog. Biophys. Mol. Biol.* **1996**, *66*, 43−80.
(19) Solomon, I.; Bloembergen, N. *J. Chem. Phys.* **1956**, *25*, 261 DOI: 10.1063/1.1742867.
(20) Cavanagh, J.; Fairbrother, W. J.; Palmer, A. G., III; Skelton, N. J.; Rance, M. *Protein NMR Spectroscopy: Principles and Practice;* Academic Press (Elsevier): Amsterdam, 2006.
(21) Srinivasan, R.; Fleming, P. J.; Rose, G. R. *Methods Enzymol.* **2004**, *383*, 48−66.
(22) George, G. N.; Pickering, I. J. *EXAFSPACK;* Stanford Synchrotron Radation Lightsource, 2000.
(23) Zabinsky, S. I.; Rehr, J. J.; Ankudinov, A.; Albers, R. C.; Eller, M. J. *Phys. Rev. B* **1995**, *52*, 2995−3009.
(24) Wang, S.; Lee, M. H.; Hausinger, R. P.; Clark, P. A.; Wilcox, D. E.; Scott, R. A. *Inorg. Chem.* **1994**, *33*, 1589−1593.
(25) Liu, W.; Thorpe, H. H. *Inorg. Chem.* **1993**, *32*, 4102−4105.
(26) Okrasa, K.; Kazlauskas, R. J. *Chem.—Eur. J.* **2006**, *12*, 1587−1596.
(27) Le, V. H.; Buscaglia, R.; Chaires, J. B.; Lewis, E. A. *Anal. Biochem.* **2013**, *434*, 233−241.
(28) Bertini, I.; Fragai, M.; Lee, Y.-M.; Luchinat, C.; Terni, B. *Angew. Chem., Int. Ed* **2004**, *43*, 2254−2256.
(29) Arnesano, F.; Banci, L.; Bertini, I.; Felli, I. C.; Luchinat, C.; Thompsett, A. R. *J. Am. Chem. Soc.* **2003**, *125*, 7200−7208.
(30) Smith, S. R.; Bencze, K. Z.; Wasiukanis, K.; Stemmler, T. L.; Benore-Parsons, M. *Open Inorg. Chem. J.* **2008**, *2*, 22−24.
(31) Kau, L. S.; Spira-Solomon, D. J.; Penner-Hahn, J. E.; Hodgson, K. O.; Solomon, E. I. *J. Am. Chem. Soc.* **1987**, *109*, 6433−6442.
(32) Leitch, S.; Bradley, M. J.; Rowe, J. L.; Chivers, P. T.; Maroney, M. J. *J. Am. Chem. Soc.* **2007**, *129*, 5085−5095.
(33) Periyannan, G. R.; Costello, A. L.; Tierney, D. L.; Yang, K.-W.; Bennett, B.; Crowder, M. W. *Biochemistry* **2005**, *45*, 1313−1320.
(34) Vallee, B. L.; Auld, D. S. *Proc. Natl. Acad. Sci. U. S. A.* **1990**, *87*, 220−224.
(35) Park, J. H.; Meriwether, B. P.; Clodfelder, P.; Cunningham, L. W. *J. Biol. Chem.* **1961**, *236*, 136−141.
(36) Tu, C.; Wynns, G. C.; Silverman, D. N. *J. Biol. Chem.* **1961**, *256*, 9468−9470.
(37) Grossoehme, N. E.; Spuches, A. M.; Wilcox, D. E. *J. Biol. Inorg. Chem.* **2010**, *15*, 1183−1191.
(38) Hong, L.; Bush, W. D.; Hatcher, L. Q.; Simon, J. *J. Phys. Chem. B* **2008**, *112*, 604−611.
(39) Quinn, C. F. *A Thermodynamic Study of Essential and Toxic Metals Binding to Proteins, Peptides and Small Molecules involved in Detoxification, Storage, and Gene Regulation;* Dartmouth University: Hanover, NH, 2009.
(40) NIST Standard Reference Datebase 46. *Technology;* National Institute of Standards and Technology, Ed.: Gaithersburg, VA, 2003.
(41) Nagaj, J.; Stokowa-Sołtys, K.; Kurowska, E.; Frączyk, T.; Jeżowska-Bojczuk, M.; Bal, W. *Inorg. Chem.* **2013**, *52*, 13927−13933.
(42) Zawisza, I.; Rózga, M.; Poznański, J.; Bal, W. *J. Inorg. Biochem.* **2013**, *129*, 58−61.
(43) DiTusa, C. A.; Christensen, T.; McCall, K. A.; Fierke, C. A.; Toone, E. J. *Biochemistry* **2001**, *40*, 5338−5344.
(44) Tarapaidze, A.; Hureau, C.; Bal, W.; Winterhalter, M.; Faller, P. *J. Biol. Inorg. Chem.* **2012**, *17*, 37−47.
(45) Irving, H.; Williams, R. J. P. *Nature* **1948**, *162*, 746−747.
(46) Zhang, Y.; Wilcox, D. E. *J. Biol. Inorg. Chem.* **2002**, *7*, 327−337.
(47) Sankararamakrishnan, R.; Verma, S.; Kumar, S. *Proteins* **2005**, *58*, 211−221.
(48) Harford, C.; Sarkar, B. *Biochem. Biophys. Res. Commun.* **1995**, *209*, 877−882.
(49) Gogineni, D. P.; Spuches, A. M.; Burns, C. S. *Inorg. Chem.* **2014**, *54*, 441−447.
(50) Sacco, C.; Skowronsky, R. A.; Gade, S.; Kenney, J. M.; Spuches, A. M. *J. Biol. Inorg. Chem.* **2012**, *17*, 531−541.
(51) Hong, L.; Carducci, T. M.; Bush, W. D.; Dudzik, C. G.; Millhauser, G. L.; Simon, J. D. *J. Phys. Chem. B* **2010**, *114*, 11261−11271.

DOI: 10.1021/acs.inorgchem.5b00057
Inorg. Chem. 2015, 54, 5671−5680

(52) Ginotra, Y. P.; Ramteke, S. N.; Srikanth, R.; Kulkarni, P. P. *Inorg. Chem.* **2012**, *51*, 7960−7962.
(53) Hureau, C.; Eury, H.; Guillot, R.; Bijani, C.; Sayen, S.; Solari, P.-L.; Guillon, E.; Faller, P.; Dorlet, P. *Chem.—Eur. J.* **2011**, *17*, 10151−10160.
(54) Minicozzi, V.; Stellato, F.; Comai, M.; Serra, M. D.; Potrich, C.; Meyer-Klaucke, W.; Morante, S. *J. Biol. Chem.* **2008**, *283*, 10784.
(55) King, R. W.; Roberts, G. C. K. *Biochemistry* **1971**, *10*, 558−565.
(56) Dehareng, D.; Dive, G. *Int. J. Mol. Sci.* **2004**, *5*, 301−332.
(57) Bhattacharya, S.; Lecomte, J. T. J. *Biophys. J.* **1997**, *73*, 3241−3256.
(58) Bertini, I.; Canti, G.; Luchinat, C.; Scozzafava, A. *J. Chem. Soc., Dalton Trans.* **1978**; DOI: 10.1039/DT9780001269.
(59) Fukada, H.; Takahashi, K. *Proteins* **1998**, *33*, 159−166.

DOI: 10.1021/acs.inorgchem.5b00057
Inorg. Chem. 2015, 54, 5671−5680